

FLORIDA STATE UNIVERSITY  
COLLEGE OF ARTS & SCIENCES

THIS IS MY TITLE:  
AND THIS IS ITS SECOND LINE

By  
JULIA REAM

A Dissertation submitted to the  
Department of Mathematics  
in partial fulfillment of the  
requirements for the degree of  
Doctor of Philosophy

2023

Julia Ream defended this dissertation on Month ##, 2023.

The members of the supervisory committee were:

Mark Sussman

Professor Co-Directing Dissertation

Marc Henry de Frahan

Professor Co-Directing Dissertation

Bryan Quaife

University Representative

Aseel Farhat

Committee Member

Sanghyun Lee

Committee Member

The Graduate School has verified and approved the above-named committee members, and certifies that the dissertation has been approved in accordance with university requirements.

Blah Blah Blah

# ACKNOWLEDGMENTS

Blah Blah Blah

# TABLE OF CONTENTS

List of Figures . . . . .	vii
List of Abbreviations . . . . .	viii
Abstract . . . . .	ix
<b>1 Introduction</b>	<b>1</b>
1.1 Mathematics of Fluid Flow . . . . .	2
1.1.1 Continuum Description of Fluids . . . . .	4
1.1.2 Equation of State . . . . .	6
1.2 Turbulence . . . . .	7
1.2.1 Historical Perspective . . . . .	8
1.2.2 Numerical Approaches . . . . .	8
1.3 Supercritical Carbon Dioxide . . . . .	8
1.3.1 Applications of Interest . . . . .	9
1.3.2 Overview of Current Numerical Landscape . . . . .	11
<b>2 Model Overview</b>	<b>13</b>
2.1 Introduction . . . . .	13
2.2 Governing Equations . . . . .	13
2.2.1 High Pressure Corrections for Transport Models . . . . .	14
2.3 Numerical Methods . . . . .	14
2.3.1 Subgrid-Scale Modeling for Large Eddy Simulation . . . . .	14
2.3.2 Piecewise Parabolic Method Overview . . . . .	15
2.3.3 Approximate Riemann Solver Details . . . . .	15
2.3.4 Time Stepping with RK2 . . . . .	15
<b>3 Simulations</b>	<b>16</b>
3.1 AMReX and Discretization . . . . .	16
3.2 Case Descriptions . . . . .	16
3.2.1 Parameter Choices . . . . .	16
3.3 Compute Time and Hardware Specifications . . . . .	16
3.4 Post-Processing Procedures . . . . .	16

<b>4</b>	<b>Results</b>	<b>17</b>
4.1	Ideal Gas Comparison . . . . .	17
4.1.1	Mean Turbulence Statistics . . . . .	17
4.2	Cross-Case Comparisons . . . . .	17
4.2.1	Axial Visuals . . . . .	17
<b>5</b>	<b>Conclusion</b>	<b>18</b>
5.1	Summary . . . . .	18
5.2	Future Work . . . . .	18
	Bibliography . . . . .	19
	Biographical Sketch . . . . .	24

# LIST OF FIGURES

1.1	Characteristic length scale of problem, $L$ , compared to mean free path of particles, $\ell$ , for a flow with large Knudsen number (left) vs. small Knudsen number (right) . . . .	3
1.2	A fluid of arbitrary volume $V$ bounded by surface $S$ with velocity $\vec{v}(\vec{x}, t)$ . A differential volume and surface area is given by $dv$ and $ds$ , respectively. $\vec{n}$ is the outward-pointing unit normal vector to the surface $S$ . . . . .	4
1.3	Example of streamlines in laminar (left) vs. turbulent (right) flow. . . . .	7
1.4	Phase diagram for Carbon Dioxide (CO <sub>2</sub> ). Critical pressure, $p_c$ , and temperature, $T_c$ , are 73.773 bar and 304.128 K, respectively. . . . .	9
1.5	Size comparison for steam vs. supercritical Carbon Dioxide (sCO <sub>2</sub> ) turbine via Echogen Power Systems LLC [29]. . . . .	10

# LIST OF ABBREVIATIONS

The following short list of abbreviations are used throughout this document.

AMR	Adaptive Mesh Refinement
CFD	Computational Fluid Dynamics
CO <sub>2</sub>	Carbon Dioxide
DNS	Direct Numerical Simulation
DOE	Department of Energy
ECP	Exascale Computing Project
EoS	equation of state
HPC	high-performance computing
LES	Large Eddy Simulation
NIST	National Institute of Standards and Technology
NREL	National Renewable Energy Laboratory
PPM	piecewise parabolic method
PR EoS	Peng-Robinson equation of state
RANS	Reynolds-Averaged Navier-Stokes
rms	root mean square
sCO <sub>2</sub>	Supercritical Carbon Dioxide
SGS	Subgrid Scale
SMD	dynamic Smagorinsky
SRK EoS	Soave-Redlich-Kwong equation of state



# ABSTRACT

Blah Blah Blah

# CHAPTER 1

## INTRODUCTION

Fluids are a vital part of everyday life - two of the most common ones being the air we breathe and the water we drink. Less obvious are all the ways even these common fluids function behind the scenes in our day to day activities. Water, for example, serves an important role in various industrial settings, proving useful in areas ranging from thermal management to energy production; steam turbines alone accounted for 45% of electricity generation in the United States in 2021 [40]. Improvements to these types of systems impact technologies across a variety of fields and are thus an important area of research. One strategy toward this end, and the primary motivator of the work presented here, is the use of supercritical fluids as the working fluid of these systems.

In order to discuss supercritical fluids further, we must first go into more detail about general fluids. A *fluid* is a large collection of mutually interacting particles (e.g. molecules, atoms, etc.) in a state of constant and chaotic motion. This results in the continuous deformation of the substance under the effects of a shearing stress. The two categories of fluids that most people are familiar with are gases and liquids. *Liquids* are (mostly) incompressible and have definite volume for a set temperature and pressure. *Gases* are compressible and do not have definite volume. A simplified distinction between the two is that both gases and liquids will conform to the shape of whatever container they are in, but gases will further spread to fill all available space present.

A *supercritical fluid* is a fluid that is held above a critical temperature and pressure, at which point the distinction between a gas and liquid phase no longer exists [14, 41]. Supercritical fluids have qualities associated with both gases and liquids yet simultaneously have features that exclude them from fully being categorized as one or the other. For example, while they have viscosities akin to gases, they have solvent capabilities associated with liquids []. Similarly, while they have densities in line with liquids, they lack surface tension []. One benefit of this duality is that supercritical fluids can be fine tuned to be more gas-like or more liquid-like depending on the application at hand. This also results in ambiguity on how to actually classify them, with some sources considering them highly compressed gases [18], expanded liquids [1], or even as their own distinctly separate phase [4]. The distinction usually lies on the specifics of the regime and the application at hand.

This work is concerned with sCO<sub>2</sub> in particular. sCO<sub>2</sub> has many beneficial features to a wide variety of industrial applications, as we will detail further in section []. Many of the applications of interest to this work involve injection technologies that require a round turbulent jet configuration within the system. While much research has gone into sCO<sub>2</sub> flows, the current landscape is lacking in turbulence of this type with the context of understanding the underlying physics relating to the flow itself. For research that does involve other supercritical turbulent jets, the regimes explored in those works typically involve transcritical fluid injection within the regime of interest or explore regions outside the scope of this work.

The goal of this work is to explore the pseudo-boiling region of the pseudo-critical zone and analyze the influence of extreme thermodynamic fluctuations on turbulence statistics within the flow field. To that end, the rest of this chapter continues as follows: first, the mathematical framework for modeling compressible Newtonian fluids is provided to form the basis of the modeling done in this dissertation. Further consideration is then given to turbulence modeling and the numerical methods developed for studying turbulence to provide insight into the quantities of interest analyzed within this dissertation and the choices of numerical methods used herein. Important applications of supercritical carbon dioxide in particular are provided to motivate the problem presented in this dissertation. Existing numerical studies on supercritical fluids are reviewed to demonstrate how this dissertation fits into the current landscape of research and to emphasize the contribution the results of this work make to the field. This chapter concludes with an outline of the dissertation, the goals of the dissertation, and the main contributions made through this work.

## 1.1 Mathematics of Fluid Flow

Scale is one of the key factors to consider when developing a mathematical description of a fluid system. For example, consider modeling flow past a satellite in the exosphere vs. the flow past a turtle in the ocean; these two mediums have vastly different characteristics and would thus require different modeling techniques. Scale is also an important concept when it comes to turbulence in particular so we will begin that discussion here with our choice in perspective for the mathematical framework of our system of interest.

From a kinetics perspective, particle motion within a fluid can be broken up into two phases: particle interaction and free flight. Average time spent in free flight,  $\langle t_f \rangle$ , is typically much greater than collision time for a given interaction,  $t_c$ . The average length traveled between collisions

is known as the mean free path,  $\ell$ . Since free flight time dominates particle interaction time, this phase determines the length scale of the kinetic description of motion. In addition to this inherent physical scale, there is also a scale associated with the resolution of the problem itself,  $L$ . These two scales are important, as the mathematical description of your model depends on how these two scales compare to one another. This comparison is related through the non-dimensional Knudsen number:

$$Kn = \frac{\ell}{L} \quad (1.1)$$

Flows with large Knudsen number ( $Kn \gg 10$ ) require modeling from the kinetic or microscopic perspective as particle interactions become sparse enough compared to the scope of the problem to require a statistical mechanics framework. On the other hand, small Knudsen number flows ( $Kn \ll 0.01$ ) have a problem scale that far exceeds the particle-level interactions present, giving way to an average overall motion within the fluid. This scale dichotomy is demonstrated with the graphic in Figure ?? For small Knudsen flows, a continuum description of the fluid is appropriate for capturing this macroscopic behavior.

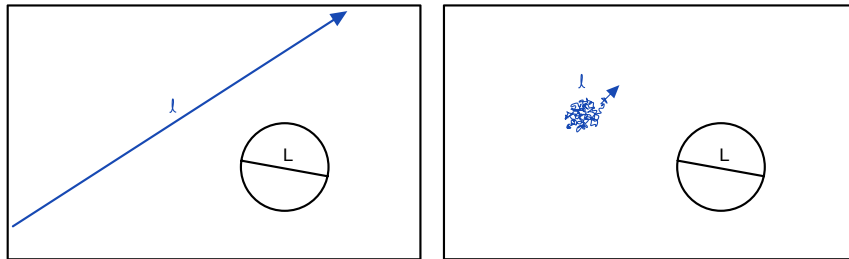


Figure 1.1: Characteristic length scale of problem,  $L$ , compared to mean free path of particles,  $\ell$ , for a flow with large Knudsen number (left) vs. small Knudsen number (right)

This work falls within the small Knudsen regime, so we will be working with the continuum description of fluids. In this section we will discuss the Navier-Stokes Equations that arise from this modeling technique and how we account for the supercritical nature of the flow through our choice of equation of state.

### 1.1.1 Continuum Description of Fluids

The continuum hypothesis assumes that the fluid has no fine structures and that it is perfectly continuous, i.e. the properties of a small subdivision are the same as other subdivisions. This allows for the approximation of physical quantities at the infinitesimal limit [19].

For example, consider a fluid with arbitrary volume  $V$  as depicted in Figure 1.2.

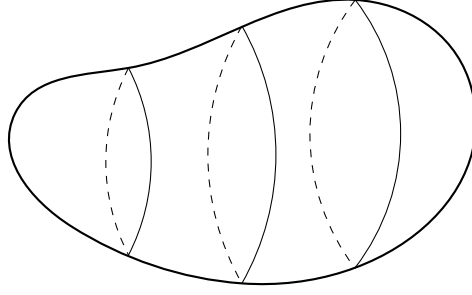


Figure 1.2: A fluid of arbitrary volume  $V$  bounded by surface  $S$  with velocity  $\vec{v}(\vec{x}, t)$ . A differential volume and surface area is given by  $dv$  and  $ds$ , respectively.  $\vec{n}$  is the outward-pointing unit normal vector to the surface  $S$ .

For a fluid with density  $\rho(\vec{x}, t)$ , mass within a small representative volume can be described with

$$\rho dv$$

Total mass in the arbitrary volume is then given by

$$\iiint_V \rho dv$$

The rate of change of mass through the volume is now

$$\begin{aligned} & \frac{d}{dt} \iiint_V \rho dv \\ &= \iiint_V \frac{\partial \rho}{\partial t} dv \end{aligned} \tag{1.2}$$

Simultaneously, overall change in mass throughout the volume can be described by the net mass flux through the surface  $S$ . Volumetric flow through a small portion of the bounding surface is given by

$$\vec{v} \cdot \vec{n} ds$$

Total mass flux through the entire surface is then

$$\iint_S \rho \vec{v} \cdot \vec{n} \, ds \quad (1.3)$$

Applying the divergence theorem to Eq. 1.3 yields the following volume integral

$$\iiint_V \nabla \cdot (\rho \vec{v}) \, dv \quad (1.4)$$

Assuming there is no additional source generating or leaking mass within the control volume, we can relate Eqs. 1.2 to 1.4 :

$$\begin{aligned} \iiint_V \frac{\partial \rho}{\partial t} \, dv &= - \iiint_V \nabla \cdot (\rho \vec{v}) \, dv \\ \iiint_V \frac{\partial \rho}{\partial t} \, dv + \iiint_V \nabla \cdot (\rho \vec{v}) \, dv &= 0 \\ \iiint_V \left( \frac{\partial \rho}{\partial t} + \nabla \cdot (\rho \vec{v}) \right) \, dv &= 0 \end{aligned} \quad (1.5)$$

Note the inclusion of the negative sign for the right side of the initial equality; in the surface integral formulation, the outward facing normal describes flux out of the volume, thus yielding a decrease in mass within the volume. Since Eq. 1.5 holds for any arbitrary volume  $V$ , the integrand must be identically equal to zero:

$$\frac{\partial \rho}{\partial t} + \nabla \cdot (\rho \vec{v}) = 0 \quad (1.6)$$

Through the continuum hypothesis and conservation of mass, we have now arrived at the continuity equation in Eq. 1.6. This specific process demonstrates an even more fundamental relationship known as a *conservation law*. More generally, for some integrated property  $\phi$ , the rate of change of  $\phi$  within a control volume must be equal to the amount of  $\phi$  lost or gained through the boundaries of the control volume plus what is created or consumed by any sinks or sources,  $s$ , within the volume (sinks having positive orientation to match the positive orientation of the outward-facing normal  $\vec{n}$ ) [].

$$\frac{\partial \phi}{\partial t} + \nabla \cdot (\phi \vec{v}) + s = 0 \quad (1.7)$$

In addition to this concept applying to conservation of mass, as was seen in this section, the idea outlined by Eq. 1.7 applies to conservation of momentum and energy within the fluid. Together, these expressions combine to form the basis of the Navier-Stokes Equations, as will be seen in more detail in chapter 2. The important takeaway from this section is that with the continuum hypothesis and fundamental laws of physics, one can adequately capture macroscopic flow behavior for the types of flows we are interested in within this work.

### 1.1.2 Equation of State

Conservation of mass, momentum, and energy gives us five equations to describe our fluid system. For compressible flows, this is not enough information to solve for all the unknowns within the system of coupled partial differential equations. A sixth equation, known as the Equation of State (EoS), must be chosen in order to close the system. The EoS relates three of the six unknowns: pressure, temperature, and density. Here we will briefly discuss some EoS options and their distinguishing characteristics in order to motivate the choice made for this work.

The simplest option available is the ideal gas EoS, which comes from the ideal gas law. This EoS relates density, pressure, and temperature in the following manner:

$$p = \frac{RT}{V_m} \quad (1.8)$$

where  $p$  is pressure,  $R$  is the universal gas constant,  $T$  is temperature, and  $V_m = \frac{V}{n}$  is the molar volume of the fluid (it is common to express density in terms of molar volume for sake of simplicity in writing the EoS with  $V$  being volume and  $n$  being the number of moles). The ideal gas EoS is fairly accurate for liquids and gases at moderate temperatures and low pressures. It fails at low temperatures and high pressures, especially near the transition region from gas to liquid. The inaccuracy noted in this region means this EoS would not be suitable for the area of interest within this study.

Cubic EoS generally provide more accuracy than the ideal gas EoS. The first cubic EoS was developed by van der Waal in 1873, modifying the ideal gas EoS to take into consideration the finite size of molecules and interactions between molecules (the ideal gas EoS only accounts for interactions with the container and treats molecules as point particles). Other cubic EoS can be thought of as modifications from this base form:

$$p = \frac{RT}{V_m - b} - \frac{a}{V_m^2} \quad (1.9)$$

where  $a$  and  $b$  are constants related to the pressure and temperature at the critical point,  $p_c$  and  $T_c$  respectively:

$$a = \frac{27(RT_c)^2}{64p_c}, \quad b = \frac{RT_c}{8p_c}$$

One of the main benefits of using a cubic EoS is that they can have comparable and sometimes even better accuracy compared to their higher order counterparts, thus reducing computational costs. However, it is important to take into consideration the regime of interest in addition to

the fluid of interest when choosing an EoS, as each one has its own pros and cons. For example, molecule polarity and density are two factors that can have a high impact in selection between the Soave-Redlich-Kwong Equation of State (SRK EoS) and Peng-Robinson Equation of State (PR EoS) alone [17].

This work uses the SRK EoS as will be more thoroughly introduced in chapter 2. It has been shown that this equation of state is fairly accurate for the parameter regime under careful consideration in this work []. This accuracy is detailed further in chapter 3 through comparisons with data from National Institute of Standards and Technology (NIST). Overall, when adequately considered, the EoS is the key avenue to incorporating specific fluid properties into the mathematical model.

## 1.2 Turbulence

In addition to the categorizing of fluid type, fluid flow can be distinguished into different types based on certain defining flow characteristics. The main two classifications of note are laminar flow and turbulent flow.

Laminar flow is denoted by fluid particles having well-defined parallel trajectories of motion, or streamlines. Streamlines do not cross, meaning adjacent layers within the fluid flow by one another with little to no mixing. From a more generalized perspective, the flow appears to be smooth. In contrast to this, turbulent flow is characterized by its unpredictable and chaotic trajectories. Streamlines do cross resulting in swirls and eddies of varying length scales which induce mixing. Turbulent flow can be qualitatively described as being rough due to this high degree of fluctuation within the velocity and pressure fields present. This generalized description is depicted in Figure 1.3.

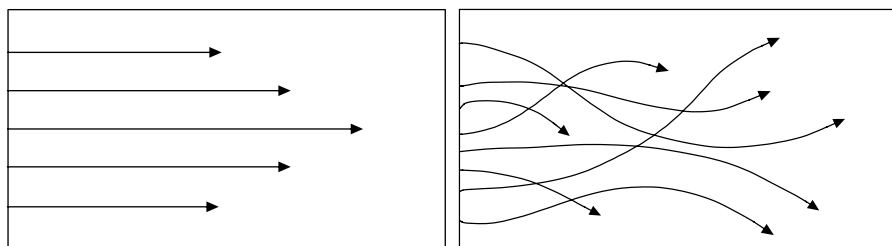


Figure 1.3: Example of streamlines in laminar (left) vs. turbulent (right) flow.



The Reynolds number is a dimensionless value that can be used to distinguish laminar flow from turbulent flow. It is defined as follows:

$$\text{Re} = \frac{\rho u L}{\mu} \quad (1.10)$$

where  $\rho$  and  $\mu$  are the density and dynamic viscosity of the fluid, respectively,  $u$  is the flow velocity, and  $L$  is a characteristic length scale associated with the given flow scenario (e.g. pipe diameter). As is demonstrated by the ratio in Equation 1.10, the Reynolds number measures the relative effects of inertial forces compared to viscous forces within a given flow scenario. A small Reynolds number signifies the dominance of viscous forces; fluid parcels moving in tandem want to “stick together,” resulting in the sheared flow and parallel trajectories seen in laminar flow. Turbulence is then characterized by a large Reynolds number, where inertial forces take precedence. Here, deviations within the laminar flow field result in lateral mixing between shear layers. This creates eddies and random trajectories that result in the chaotic motion of turbulent flow.

This work focuses on the turbulent round jet and its associated dynamics in the context of supercritical fluids. The remainder of this section details a brief historical overview of turbulence modeling and numerical methods developed for studying turbulence in order to motivate the modeling and numerical choices made within this work.

### 1.2.1 Historical Perspective

This is a brief history of turbulence study from a mathematics perspective.

### 1.2.2 Numerical Approaches

These are some of the numerical approaches in use, including what we use and why we use it.

## 1.3 Supercritical Carbon Dioxide

As mentioned earlier, supercritical fluids have many qualities that make them desirable as working fluids in a variety of systems. We now shift our focus to one particular fluid of interest: Carbon Dioxide (CO<sub>2</sub>). As seen in the phase diagram of Figure 1.4, the critical temperature,  $T_c$ , and critical pressure,  $p_c$ , of CO<sub>2</sub> are 304.128 K and 73.773 bar. The critical temperature and pressure of CO<sub>2</sub> is fairly easy to attain, making it a strong candidate for systems with high thermal outputs. Additionally, sCO<sub>2</sub> has a relatively low toxicity and environmental impact [], and is chemically stable, non-flammable, and readily available []. For these reasons, sCO<sub>2</sub> is a highly

coveted alternative working fluid in many different applications, and is one of the most widely used supercritical fluids along with water [14].

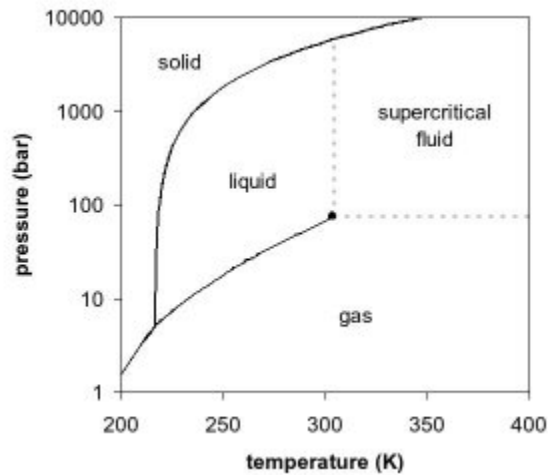


Figure 1.4: Phase diagram for Carbon Dioxide (CO<sub>2</sub>). Critical pressure,  $p_c$ , and temperature,  $T_c$ , are 73.773 bar and 304.128 K, respectively.

In the next part of this section, we will explore some applications of sCO<sub>2</sub> in which the turbulent round jet configuration is used. Then we will go through a brief review of recent studies involving sCO<sub>2</sub>, and more generally supercritical turbulent jets, in order to demonstrate where this work fits in among current research. Finally, we outline the structure of the remainder of the dissertation.

### 1.3.1 Applications of Interest

One of the key applications of interest that motivates this work is the use of sCO<sub>2</sub> as the working fluid in advanced cycles for power generation. sCO<sub>2</sub> has shown promise as a working fluid for both indirect cycle and direct-firing cycles [46, 47]. One example of indirect cycle improvement uses sCO<sub>2</sub> in place of water for the conventional steam-Rankine cycle. An example of where these types of configurations may prove useful is in managing thermal runoff from existing coal and natural gas combustion processes [46]. Compared to steam, sCO<sub>2</sub> is less corrosive, more thermally stable, and has increased power density. The critical point of CO<sub>2</sub> is easily accessible, and once achieved, allows for the use of a single phase fluid design, leading to a simplified and more compact turbine (see Figure 1.5). Ultimately, this also allows for lower operation and maintenance costs [10]. The

benefits of using sCO<sub>2</sub> turbines over the traditional steam design has been highly researched and has only seen an increase in momentum for implementation [9, 13, 11, 29].

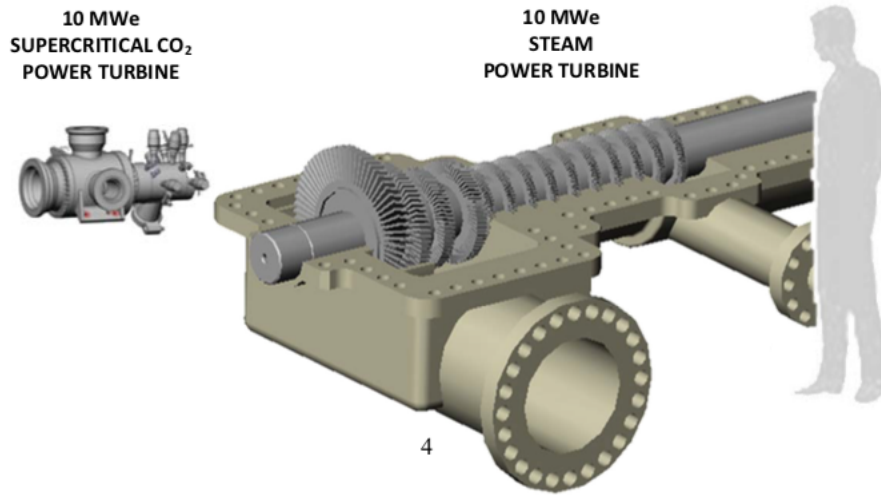


Figure 1.5: Size comparison for steam vs. sCO<sub>2</sub> turbine via Echogen Power Systems LLC [29].

An example of direct-firing cycles that use sCO<sub>2</sub> include the Allam cycle [2]. When compared to the conventional Brayton cycle, studies show that the Allam cycle has much higher efficiency [12, 3]. Additionally, the carbon footprint for the Allam cycle is virtually zero, allowing for CO<sub>2</sub> produced from the system to be stored underground or used elsewhere, aiding in carbon sequestration efforts [15]. This two-for-one benefit of using sCO<sub>2</sub>-based cycles such as the Allam cycle has spurred much research [44, 5] and development [34] into related technologies.

Of particular importance to these applications is the round turbulent jet, as this is a major component of many injection technologies. The high densities associated with the liquid-like aspect of supercritical fluids coupled with the relatively low gas-like viscosity associated with them typically results in a high Reynolds flow, often resulting in a turbulent system. The turbulence physics of these jets is crucial in developing machinery for these systems. Current experimental research is mainly application oriented. Research into the sCO<sub>2</sub> jet's rock breaking ability has been of primary importance to Enhanced Geothermal Systems (EGS) applications [31, 32, 24, 38, 23], with additional focus being given to pipeline leakage and flow dynamics upon wall impact [43, 42], which unfortunately does not explore the underlying turbulence statistics of the flow. Chemical engineering design aspects of sCO<sub>2</sub> injection are more focused on solubility dynamics as opposed to

turbulence [20, 21]. Other experiments focus on similar application specific quantities of interest, such as heat transfer and mixing, which is related in part to the turbulence dynamics [48], but they also note the difficulty in experimental design for investigating these aspects of the flow under the conditions needed to replicate those in real applications [20]. Thus, numerical simulations are necessary to further explore the turbulence statistics of these flows.

### 1.3.2 Overview of Current Numerical Landscape

Much research has gone into the development of appropriate numerical methods for such investigations, though challenges arise due to the lack of experimental data for use in model validation. Studies using direct numerical simulation (DNS) have been implemented to help establish benchmark test cases for other types of numerical schemes. Ruiz et al. use 2D DNS to simulate a mixing layer created by two streams of supercritical Oxygen and gaseous Nitrogen, using two different computational fluid dynamics (CFD) solvers to add confidence to their results [35]. A 3D DNS is used by Ries et al. to simulate a round Nitrogen jet for comparison with experimental data produced by Mayer et al. [33]. However, this study requires a reduction in Reynolds number from  $1.62 \times 10^5$ , based on the injection diameter, to 5300 in order to feasibly execute the computations. Li also utilizes a low Reynolds number of 1750 to study a round turbulent sCO<sub>2</sub> jet with a preconditioning scheme [22]. The Reynolds-averaged Navier-Stokes (RANS) approach has also been implemented utilizing theory from the ideal gas case [25], but with the goal of ascertaining a more general understanding of why specifically sCO<sub>2</sub>'s rock-breaking ability is better than that of water. In order to maintain a high Reynolds flow and better capture the effects of the supercritical nature of the fluid on the turbulence dynamics, the use of large eddy simulation (LES) has been explored. The impact of subgrid scale (SGS) models in capturing transcritical and supercritical dynamics of cryogenic Nitrogen have been analyzed through comparison with the Mayer et al. experiment and highly accurate NIST data [30, 49, 50, 28, 45]. Schmitt et al. does a similar investigation using LES, then extending their investigation to include sCO<sub>2</sub> after validation with the Mayer et al. data. [37] However, this investigation uses low-pressure jets and does note the SGS models might need additional contributions to handle non-linearities and the pressure regime. While many of these investigations note that SGS models may need modification to deal with supercritical flows [37, 30, 28, 49], it is noted by Muller et al. that given a sufficiently fine grid, the influence of SGS modeling and numerical flux discretization is essentially limited to second-order moments [28]. Thus, we will be using the compressible version of the dynamic Smagorinsky SGS closures for our

investigation, with further consideration of any influence of SGS model on our quantities of interest being noted later on. While much of the literature thus far has explored the impact of different numerical methods on modeling supercritical fluid flows and has aimed to strengthen the validity of these simulations in spite of the lack of experimental data available in the current landscape, a general consensus has still not been reached on how the supercritical nature of these fluids impacts the turbulence physics of these models. Thus, there remain open questions for understanding the fundamental flow behavior of turbulent jets in a supercritical environment, especially near the supercritical point, where both experimental and numerical investigations are still a challenge.

# CHAPTER 2

## MODEL OVERVIEW

### 2.1 Introduction

Chapter 1 introduced the general mathematical framework needed for modeling fluid flow.

### 2.2 Governing Equations

We consider the three-dimensional compressible Navier-Stokes equations:

$$\begin{aligned}\frac{\partial \rho}{\partial t} + \frac{\partial}{\partial x_j} (\rho u_j) &= 0, \\ \frac{\partial}{\partial t} (\rho u_i) + \frac{\partial}{\partial x_j} (\rho u_i u_j + p \delta_{ij} - \sigma_{ij}) &= 0, \\ \frac{\partial}{\partial t} (\rho E) + \frac{\partial}{\partial x_j} ((\rho E + p) u_j + q_j - \sigma_{ij} u_i) &= 0\end{aligned}\tag{2.1}$$

where  $\rho$  is the density,  $u_j$  is the velocity for the  $x_j$  direction,  $p$  is the pressure,  $E = e + \frac{u_i u_i}{2}$  is the total energy,  $e = c_v T$  is the internal energy,  $T$  is the temperature, and  $c_v$  is the heat capacity at constant volume. Additionally, the diffusive fluxes are

$$\sigma_{ij} = 2\mu S_{ij} - \frac{2}{3}\mu \delta_{ij} S_{kk} q_j = -k \frac{\partial T}{\partial x_j}\tag{2.2}$$

where  $S_{ij} = \frac{1}{2} \left( \frac{\partial u_i}{\partial x_j} + \frac{\partial u_j}{\partial x_i} \right)$  is the strain-rate tensor,  $\mu$  is the dynamic viscosity, and  $k$  is the thermal conductivity. External forces such as gravity are not included in this study. Chung's high pressure correction for viscosity and thermal conductivity are included for the transport variables  $\mu$  and  $k$  [6]. The system is closed using the SRK EoS [39] to relate pressure, density, and temperature as follows:

$$p = \frac{RT}{V_m - b} - \frac{a\alpha}{V_m(V_m + b)}\tag{2.3}$$

$$a = \frac{0.42747 R^2 T_c^2}{P_c}\tag{2.4}$$

$$b = \frac{0.08664 R T_c}{P_c}\tag{2.5}$$

$$\alpha = \left( 1 + (0.48508 + 1.55171\omega - 0.15613\omega^2) (1 - T_r^{0.5}) \right)^2\tag{2.6}$$

$$T_r = \frac{T}{T_c}\tag{2.7}$$

where  $R$  is the ideal gas constant,  $T$  is the absolute temperature,  $V_m$  is the molar volume of the species,  $T_c$  and  $P_c$  are the critical temperature and pressure of the species, respectively, and  $\omega$  is the acentric factor of the species. Additionally,  $a$ ,  $b$ , and  $\alpha$  are all species-specific parameters calculated via equations 2.4, 2.5, and 2.6. All cases are run with a single species, that being CO<sub>2</sub>.

### 2.2.1 High Pressure Corrections for Transport Models

## 2.3 Numerical Methods

To discretize and evolve the system of partial differential equations given in 2.1, including the LES SGS terms, we use *PeleC*, a compressible hydrodynamics code for reacting flows that leverages *AMReX* for adaptive mesh refinement (AMR) [1]. *PeleC* is a highly scalable code for heterogeneous architectures that is being developed as part of the Exascale Computing Project (ECP) through the Department of Energy (DOE). It leverages the *PelePhysics* library for complex physics, including chemical reactions, non-ideal EoS, and high fidelity transport models. For spatial discretization, *PeleC* contains a few variations of the general piecewise parabolic method (PPM) originally derived by Colella and Woodward [7]. We utilize a variation that allows for extrema preservation in the presence of steep gradients [27, 8]. For time discretization, a second order Runge-Kutta scheme is used, and the time step is dynamically limited using a Courant number of 0.9.

### 2.3.1 Subgrid-Scale Modeling for Large Eddy Simulation

We use the dynamic Smagorinsky (SMD) LES model for compressible flow as described by Martín, Piomelli, and Graham [26]. In this context, the compressible Navier-Stokes equations 2.1 should be interpreted in their Favre-filtered form, where, in this work, the grid provides the implicit filtering of the equations. The SGS stress tensor,  $\tau_{ij}$ , is included in the diffusive fluxes and is calculated as follows:

$$\begin{aligned}\tau_{ij} - \frac{\delta_{ij}}{3}\tau_{kk} &= -C_s^2 2\bar{\Delta}^2 \bar{\rho} |\tilde{S}| \left( \tilde{S}_{ij} - \frac{\delta_{ij}}{3} \tilde{S}_{kk} \right) = C_s^2 \alpha_{ij}, \\ \tau_{kk} &= C_I 2\bar{\rho} \bar{\Delta}^2 |\tilde{S}|^2 = C_I \alpha\end{aligned}\tag{2.8}$$

where  $\bar{\cdot}$  denotes the filtered variables,  $\tilde{\cdot} = \bar{\rho} \cdot / \bar{\rho}$  is the Favre-filter operation, with  $\bar{\Delta}$  being the filter width associated with the smallest scale retained by the filtering operation ( $\bar{\Delta}$  is the grid spacing for our cases). Additionally,  $|\tilde{S}| = (2\tilde{S}_{ij}\tilde{S}_{ij})^{1/2}$ . The two model coefficients are calculated as follows:

$$C = C_s^2 = \frac{\langle \mathcal{L}_{ij} M_{ij} \rangle}{\langle M_{kl} M_{kl} \rangle}, \quad C_I = \frac{\langle \mathcal{L}_{kk} \rangle}{\langle \beta - \hat{\alpha} \rangle}\tag{2.9}$$

where the Germano identity,  $\mathcal{L}_{ij} = T_{ij} - \widehat{\tau}_{ij}$ , is used to relate the SGS stress tensor to the “resolved turbulent stresses”,  $\mathcal{L}_{ij} = \left( \widehat{\rho u_i \rho u_j} / \widehat{\rho} \right) - \widehat{\rho u_i \rho u_j} / \widehat{\rho}$ , and the subtest stresses,  $T_{ij} = \widehat{\rho u_i \rho u_j} - \widehat{\rho u_i \rho u_j}$  [16]. In this relationship, a hat denotes quantities associated with a test filter  $\widehat{G}$  which has a characteristic length of  $\widehat{\Delta}$ . The breve denotes filtered quantities using  $\widehat{G}$ . Additionally, we have  $\beta_{ij} = -2\widehat{\Delta}^2 \widehat{\rho} |\widetilde{S}| \left( \widetilde{S}_{ij} - \delta_{ij} \widetilde{S}_{kk}/3 \right)$ ,  $M_{ij} = \beta_{ij} - \widehat{\alpha}_{ij}$ , and  $\beta = 2\widehat{\Delta}^2 \widehat{\rho} |\widetilde{S}|^2$ . The turbulent Prandtl number,  $Pr_T$ , is also calculated dynamically as noted in [26]:

$$Pr_T = \frac{C \langle T_k T_k \rangle}{\langle \mathcal{K}_j T_j \rangle} \quad (2.10)$$

where

$$T_j = -\widehat{\Delta}^2 \widehat{\rho} |\widetilde{S}| \frac{\partial \widetilde{T}}{\partial x_j} + \widehat{\Delta}^2 \widehat{\rho} |\widetilde{S}| \frac{\partial \widetilde{T}}{\partial x_j}, \quad \mathcal{K}_j = \left( \frac{\widehat{\rho u_j \rho T}}{\widehat{\rho}} \right) - \frac{\widehat{\rho u_j \rho T}}{\widehat{\rho}}. \quad (2.11)$$

For our simulations, we implement the three point box filter as described in [36] with a filter-grid, ratio of 2, i.e.  $\widehat{\Delta} = 2\overline{\Delta}$ .

As noted previously, the choice of SGS modeling is important in accurately capturing the turbulence statistics of the system. Müller et al. found that while the choice in thermodynamic modeling is crucial in capturing first-order moments, the effects SGS modeling is limited to second-order moments [28]. Therefore, our conclusions relating to the turbulence dynamics will be unaffected. That being said, [28] also notes that the choice in SGS model and numerical flux discretization had a larger than expected effect on resolved Reynolds stress profiles. Specifically, the constant Smagorinsky model yielded decaying fluctuation magnitudes during early evolution, resulting in the transition to a fully turbulent mixing zone to start from lower turbulence levels. However, this did agree with the jet break-up location inferred from mean density profiles, which were shifted slightly downstream by comparison to other SGS models. These relationships will be taken into consideration for this study as well and noted in the discussion of Reynolds stress profiles.

### 2.3.2 Piecewise Parabolic Method Overview

### 2.3.3 Approximate Riemann Solver Details

### 2.3.4 Time Stepping with RK2



# **CHAPTER 3**

## **SIMULATIONS**

### **3.1 AMReX and Discretization**

### **3.2 Case Descriptions**

#### **3.2.1 Parameter Choices**

### **3.3 Compute Time and Hardware Specifications**

### **3.4 Post-Processing Procedures**

## CHAPTER 4

### RESULTS

#### 4.1 Ideal Gas Comparison

##### 4.1.1 Mean Turbulence Statistics

#### 4.2 Cross-Case Comparisons

##### 4.2.1 Axial Visuals

# **CHAPTER 5**

## **CONCLUSION**

- 5.1 Summary**
- 5.2 Future Work**

# BIBLIOGRAPHY

- [1] Salonika Aggarwal and Marko Hakovirta. “Supercritical Carbon dioxide: Adequately Sole Solvent.” In: *American Journal of Engineering, Science and Technology* 10 (2021), pp. 46–61. URL: <https://journalsonline.org/american-journal-of-engineering-science-and-technology/pdfs/volume-10/4.pdf>.
- [2] Rodney John Allam, Miles Palmer, Glenn William Brown, et al. *System and method for high efficiency power generation using a carbon dioxide circulating working fluid*. US Patent 8,596,075. Dec. 2013.
- [3] Rodney Allam et al. “Demonstration of the Allam Cycle: An Update on the Development Status of a High Efficiency Supercritical Carbon Dioxide Power Process Employing Full Carbon Capture.” In: *Energy Procedia* 114 (2017). 13th International Conference on Greenhouse Gas Control Technologies, GHGT-13, 14-18 November 2016, Lausanne, Switzerland, pp. 5948–5966. ISSN: 1876-6102. DOI: <https://doi.org/10.1016/j.egypro.2017.03.1731>. URL: <https://www.sciencedirect.com/science/article/pii/S187661021731932X>.
- [4] D.T. Banuti. “Crossing the Widom-line - Supercritical pseudo-boiling.” In: *The Journal of Supercritical Fluids* 98 (2015), pp. 12–16. ISSN: 0896-8446. DOI: <https://doi.org/10.1016/j.supflu.2014.12.019>. URL: <https://www.sciencedirect.com/science/article/pii/S0896844614004306>.
- [5] Wen Chan et al. “Exergoeconomic analysis and optimization of the Allam cycle with liquefied natural gas cold exergy utilization.” In: *Energy Conversion and Management* 235 (2021), p. 113972. ISSN: 0196-8904. DOI: <https://doi.org/10.1016/j.enconman.2021.113972>. URL: <https://www.sciencedirect.com/science/article/pii/S0196890421001485>.
- [6] T.H. Chung et al. “Generalized multiparameter correlation for nonpolar and polar fluid transport properties.” In: *Ind. Eng. Chem. Res.* 27 (1988), pp. 671–679.
- [7] P. Colella and Paul R. Woodward. “The Piecewise Parabolic Method (PPM) for Gas-Dynamical Simulations.” In: *Journal of Computational Physics* 54 (Sept. 1984), pp. 174–201. DOI: [10.1016/0021-9991\(84\)90143-8](https://doi.org/10.1016/0021-9991(84)90143-8).
- [8] Phillip Colella and Michael D. Sekora. “A limiter for PPM that preserves accuracy at smooth extrema.” In: *Journal of Computational Physics* 227.15 (2008), pp. 7069–7076. ISSN: 0021-9991. DOI: <https://doi.org/10.1016/j.jcp.2008.03.034>. URL: <http://www.sciencedirect.com/science/article/pii/S0021999108001435>.
- [9] Francesco Crespi et al. “Supercritical carbon dioxide cycles for power generation: A review.” In: *Applied Energy* 195 (2017), pp. 152–183. ISSN: 0306-2619. DOI: <https://doi.org/10.1016/j.apenergy.2017.02.048>. URL: <http://www.sciencedirect.com/science/article/pii/S0306261917301915>.

- [10] Edward Dodge. *Supercritical Carbon Dioxide Power Cycles Starting to Hit the Market*. <https://breakingenergy.com/2014/11/24/supercritical-carbon-dioxide-power-cycles-starting-to-hit-the-market/>. Accessed: 2019-08-08. 2014.
- [11] Edward Dodge. *Supercritical Carbon Dioxide Power Cycles Starting to Hit the Market*. 2014. URL: <https://breakingenergy.com/2014/11/24/supercritical-carbon-dioxide-power-cycles-starting-to-hit-the-market/>.
- [12] Emad Dokhaee et al. "Simulation of the Allam cycle with carbon dioxide working fluid and comparison with Brayton cycle." In: *International Journal of Energy and Environmental Engineering* 12.3 (2021), pp. 543–550. DOI: [10.1007/s40095-021-00401-4](https://doi.org/10.1007/s40095-021-00401-4). URL: <https://doi.org/10.1007/s40095-021-00401-4>.
- [13] V. Dostal, M.J. Driscoll, and P. Hejzlar. "A Supercritical Carbon Dioxide Cycle for Next Generation Nuclear Reactors." PhD thesis. MIT, 2004.
- [14] *Explore, use, make the most of supercritical fluids*. <http://www.supercriticalfluid.org/Supercritical-fluids.146.0.html>. Accessed: 2019-08-08. 2009.
- [15] Dan Fernandes et al. "Process and Carbon Footprint Analyses of the Allam Cycle Power Plant Integrated with an Air Separation Unit." In: *Clean Technologies* 1.1 (2019), pp. 325–340. ISSN: 2571-8797. DOI: [10.3390/cleantechnol1010022](https://doi.org/10.3390/cleantechnol1010022). URL: <https://www.mdpi.com/2571-8797/1/1/22>.
- [16] M. Germano. "Turbulence: the filtering approach." In: *Journal of Fluid Mechanics* 238 (1992), 325?336. DOI: [10.1017/S0022112092001733](https://doi.org/10.1017/S0022112092001733).
- [17] Mehdi Ghanbari, Mahdi Ahmadi, and Asghar Lashanizadegan. "A comparison between Peng-Robinson and Soave-Redlich-Kwong cubic equations of state from modification perspective." In: *Cryogenics* 84 (2017), pp. 13–19. ISSN: 0011-2275. DOI: <https://doi.org/10.1016/j.cryogenics.2017.04.001>. URL: <https://www.sciencedirect.com/science/article/pii/S0011227516303538>.
- [18] R. P. Gordon. "A supercritical phase separation: The gas-gas equilibrium." In: *Journal of Chemical Education* 49.4 (1972), p. 249. DOI: [10.1021/ed049p249](https://doi.org/10.1021/ed049p249). eprint: <https://doi.org/10.1021/ed049p249>. URL: <https://doi.org/10.1021/ed049p249>.
- [19] Nikolaos D. Katopodes. "Chapter 1 - Basic Concepts." In: *Free-Surface Flow*. Ed. by Nikolaos D. Katopodes. Butterworth-Heinemann, 2019, pp. 2–98. ISBN: 978-0-12-815489-2. DOI: <https://doi.org/10.1016/B978-0-12-815489-2.00001-0>. URL: <https://www.sciencedirect.com/science/article/pii/B9780128154892000010>.
- [20] Imane Ghaleb Khalil. "Free-Jet Expansion of Supercritical CO<sub>2</sub>." PhD thesis. University of California, San Diego, 2003.

- [21] A. V. Lazarev and K. A. Tatarenko. “Gas dynamic model of the expansion of a supercritical carbon dioxide pulse jet: A self-similar solution.” In: *Russian Journal of Physical Chemistry B* 10.8 (2016), pp. 1248–1255. DOI: [10.1134/S1990793116080145](https://doi.org/10.1134/S1990793116080145). URL: <https://doi.org/10.1134/S1990793116080145>.
- [22] Hua-Guang Li, Xi-Yun Lu, and Vigor Yang. “A numerical study of fluid injection and mixing under near-critical conditions.” In: *Acta Mechanica Sinica* 28.3 (June 2012), pp. 559–571. ISSN: 1614-3116. DOI: [10.1007/s10409-012-0035-5](https://doi.org/10.1007/s10409-012-0035-5). URL: <https://doi.org/10.1007/s10409-012-0035-5>.
- [23] Mukun Li et al. “Comparative simulation research on the stress characteristics of supercritical carbon dioxide jets, nitrogen jets and water jets.” In: *Engineering Applications of Computational Fluid Mechanics* 11.1 (2017), pp. 357–370. DOI: [10.1080/19942060.2017.1293565](https://doi.org/10.1080/19942060.2017.1293565). eprint: <https://doi.org/10.1080/19942060.2017.1293565>. URL: <https://doi.org/10.1080/19942060.2017.1293565>.
- [24] Mukun Li et al. “Influences of Supercritical Carbon Dioxide Jets on Damage Mechanisms of Rock.” In: *Arabian Journal for Science and Engineering* 43.5 (May 2018), pp. 2641–2658. ISSN: 2191-4281. DOI: [10.1007/s13369-017-2984-2](https://doi.org/10.1007/s13369-017-2984-2). URL: <https://doi.org/10.1007/s13369-017-2984-2>.
- [25] Q Lv et al. “Numerical investigation on the expansion of supercritical carbon dioxide jet.” In: *IOP Conference Series: Materials Science and Engineering* 52.7 (Dec. 2013), p. 072011. DOI: [10.1088/1757-899x/52/7/072011](https://doi.org/10.1088/1757-899x/52/7/072011). URL: <https://doi.org/10.1088/1757-899x/52/7/072011>.
- [26] M. Martín, Ugo Piomelli, and Graham Candler. “Subgrid-Scale Models for Compressible Large-Eddy Simulations.” In: *Theoretical and Computational Fluid Dynamics* 13 (Feb. 2000), pp. 361–376.
- [27] G.H. Miller and P. Colella. “A Conservative Three-Dimensional Eulerian Method for Coupled Solid-Fluid Shock Capturing.” In: *Journal of Computational Physics* 183.1 (2002), pp. 26–82. ISSN: 0021-9991. DOI: <https://doi.org/10.1006/jcph.2002.7158>. URL: <http://www.sciencedirect.com/science/article/pii/S0021999102971585>.
- [28] Hagen Müller et al. “Large-eddy simulation of nitrogen injection at trans- and supercritical conditions.” In: *Physics of Fluids* 28.1 (2016), p. 015102. DOI: [10.1063/1.4937948](https://doi.org/10.1063/1.4937948). eprint: <https://doi.org/10.1063/1.4937948>. URL: <https://doi.org/10.1063/1.4937948>.
- [29] Michael Persichilli et al. “Supercritical CO<sub>2</sub> Power Cycle Developments and Commercialization: Why sCO<sub>2</sub> can Displace Steam.” In: *Power-Gen India & Central Asia*. 2012.
- [30] X. Petit et al. “Large-eddy simulation of supercritical fluid injection.” In: *The Journal of Supercritical Fluids* 84 (2013), pp. 61–73. ISSN: 0896-8446. DOI: <https://doi.org/10.1016/j.supflu.2013.09.011>. URL: <http://www.sciencedirect.com/science/article/pii/S0896844613003239>.

- [31] Karsten Pruess. *Enhanced Geothermal Systems (EGS) comparing water with CO<sub>2</sub> as heat transmission fluids*. Tech. rep. Lawrence Berkeley National Laboratory, 2007.
- [32] Karsten Pruess and Mohamed Azaroual. “ON THE FEASIBILITY OF USING SUPERCRITICAL CO<sub>2</sub> AS HEAT TRANSMISSION FLUID IN AN ENGINEERED HOT DRY ROCK GEOTHERMAL SYSTEM.” In: *Thirty-First Workshop on Geothermal Reservoir Engineering*. 2006.
- [33] Florian Ries et al. “Numerical analysis of turbulent flow dynamics and heat transport in a round jet at supercritical conditions.” In: *International Journal of Heat and Fluid Flow* 66 (Aug. 2017), pp. 172–184. DOI: [10.1016/j.ijheatfluidflow.2017.06.007](https://doi.org/10.1016/j.ijheatfluidflow.2017.06.007).
- [34] 8 Rivers. *THE ALLAM-FETVEDT CYCLE*. 2023. URL: <https://8rivers.com/portfolio/the-allam-fetvedt-cycle-and-net-power/>.
- [35] Anthony Ruiz et al. “Numerical Benchmark for High-Reynolds-Number Supercritical Flows with Large Density Gradients.” In: *AIAA Journal* 54 (Nov. 2015), pp. 1445–1460. ISSN: 0001-1452.
- [36] P. Sagaut and R. Grohens. “Discrete filters for large eddy simulation.” In: *International Journal for Numerical Methods in Fluids* 31.8 (1999), pp. 1195–1220. DOI: [10.1002/\(SICI\)1097-0363\(19991230\)31:8<1195::AID-FLD914>3.0.CO;2-H](https://doi.org/10.1002/(SICI)1097-0363(19991230)31:8<1195::AID-FLD914>3.0.CO;2-H).
- [37] Thomas Schmitt et al. “Large-Eddy Simulation of Supercritical-Pressure Round Jets.” In: *AIAA Journal* 48.9 (2010), pp. 2133–2144. DOI: [10.2514/1.J050288](https://doi.org/10.2514/1.J050288). eprint: <https://doi.org/10.2514/1.J050288>. URL: <https://doi.org/10.2514/1.J050288>.
- [38] Huaizhong Shi et al. “Design of experimental setup for supercritical CO<sub>2</sub> jet under high ambient pressure conditions.” In: *Review of Scientific Instruments* 87.12 (2016), p. 125115. DOI: [10.1063/1.4972885](https://doi.org/10.1063/1.4972885). eprint: <https://doi.org/10.1063/1.4972885>. URL: <https://doi.org/10.1063/1.4972885>.
- [39] Giorgio Soave. “Equilibrium constants from a modified Redlich-Kwong equation of state.” In: *Chemical Engineering Science* 27.6 (1972), pp. 1197–1203. ISSN: 0009-2509. DOI: [https://doi.org/10.1016/0009-2509\(72\)80096-4](https://doi.org/10.1016/0009-2509(72)80096-4). URL: <http://www.sciencedirect.com/science/article/pii/0009250972800964>.
- [40] U.S. Energy Information Administration - EIA - independent statistics and analysis. *Electricity Explained: How electricity is generated*. Nov. 2022. URL: <https://www.eia.gov/energyexplained/electricity/how-electricity-is-generated.php> (visited on 02/19/2023).
- [41] “Supercritical fluid.” In: *Chemical Business* 28.6 (2014), pp. 39–44. ISSN: 09703136. URL: <https://login.proxy.lib.fsu.edu/login?url=http://search.ebscohost.com/login.aspx?direct=true&db=f5h&AN=97302089&site=eds-live&scope=site>.

- [42] Cailin Wang et al. “Experimental study on dispersion behavior during the leakage of high pressure CO<sub>2</sub> pipelines.” In: *Experimental Thermal and Fluid Science* 105 (2019), pp. 77–84. ISSN: 0894-1777. DOI: <https://doi.org/10.1016/j.expthermflusci.2019.03.014>. URL: <http://www.sciencedirect.com/science/article/pii/S0894177719300974>.
- [43] Hai-zhu WANG et al. “Flow field simulation of supercritical carbon dioxide jet: Comparison and sensitivity analysis.” In: *Journal of Hydrodynamics, Ser. B* 27.2 (2015), pp. 210–215. ISSN: 1001-6058. DOI: [https://doi.org/10.1016/S1001-6058\(15\)60474-7](https://doi.org/10.1016/S1001-6058(15)60474-7). URL: <http://www.sciencedirect.com/science/article/pii/S1001605815604747>.
- [44] Song Wang et al. “New Conceptual Design of an Integrated Allam-Cycle Power Complex Coupling Air Separation Unit and Ammonia Plant.” In: *Industrial & Engineering Chemistry Research* 60.49 (2021), pp. 18007–18017. DOI: [10.1021/acs.iecr.1c02478](https://doi.org/10.1021/acs.iecr.1c02478). eprint: <https://doi.org/10.1021/acs.iecr.1c02478>. URL: <https://doi.org/10.1021/acs.iecr.1c02478>.
- [45] Wu Wei, Maozhao Xie, and Ming Jia. “Large eddy simulation of fluid injection under trans-critical and supercritical conditions.” In: *Numerical Heat Transfer, Part A: Applications* 70.8 (2016), pp. 870–886. DOI: [10.1080/10407782.2016.1214485](https://doi.org/10.1080/10407782.2016.1214485). eprint: <https://doi.org/10.1080/10407782.2016.1214485>. URL: <https://doi.org/10.1080/10407782.2016.1214485>.
- [46] N.T. Weiland et al. “12 - Fossil energy.” In: *Fundamentals and Applications of Supercritical Carbon Dioxide (sCO<sub>2</sub>) Based Power Cycles*. Ed. by Klaus Brun, Peter Friedman, and Richard Dennis. Woodhead Publishing, 2017, pp. 293–338. ISBN: 978-0-08-100804-1. DOI: <https://doi.org/10.1016/B978-0-08-100804-1.00012-8>. URL: <https://www.sciencedirect.com/science/article/pii/B9780081008041000128>.
- [47] Martin T. White et al. “Review of supercritical CO<sub>2</sub> technologies and systems for power generation.” In: *Applied Thermal Engineering* 185 (2021), p. 116447. ISSN: 1359-4311. DOI: <https://doi.org/10.1016/j.applthermaleng.2020.116447>. URL: <https://www.sciencedirect.com/science/article/pii/S1359431120339235>.
- [48] Jung Yul Yoo. “The Turbulent Flows of Supercritical Fluids with Heat Transfer.” In: *Annual Review of Fluid Mechanics* 45.1 (2013), pp. 495–525. DOI: [10.1146/annurev-fluid-120710-101234](https://doi.org/10.1146/annurev-fluid-120710-101234). eprint: <https://doi.org/10.1146/annurev-fluid-120710-101234>. URL: <https://doi.org/10.1146/annurev-fluid-120710-101234>.
- [49] NAN ZONG and VIGOR YANG\*. “CRYOGENIC FLUID JETS AND MIXING LAYERS IN TRANSCRITICAL AND SUPERCRITICAL ENVIRONMENTS.” In: *Combustion Science and Technology* 178.1-3 (2006), pp. 193–227. DOI: [10.1080/00102200500287613](https://doi.org/10.1080/00102200500287613). eprint: <https://doi.org/10.1080/00102200500287613>. URL: <https://doi.org/10.1080/00102200500287613>.
- [50] Nan Zong et al. “A numerical study of cryogenic fluid injection and mixing under supercritical conditions.” In: *Physics of Fluids* 16.12 (2004), pp. 4248–4261. DOI: [10.1063/1.1795011](https://doi.org/10.1063/1.1795011). eprint: <https://doi.org/10.1063/1.1795011>. URL: <https://doi.org/10.1063/1.1795011>.



# BIOGRAPHICAL SKETCH

This is my biography.